

NASA TM 56047

A STUDY OF THE EFFECT OF RADICAL LOAD DISTRIBUTIONS
ON CALIBRATED STRAIN GAGE LOAD EQUATIONS

Jerald M. Jenkins and Albert E. Kuhl

July 1977

NASA high-number Technical Memorandums are issued to provide rapid transmittal of technical information from the researcher to the user. As such, they are not subject to the usual NASA review process.

NASA Dryden Flight Research Center
Edwards, California 93523

| | | | | | |
|---|--|--|--|---|--|
| 1. Report No. NASA TM 56047 | | 2. Government Accession No. | | 3. Recipient's Catalog No. | |
| 4. Title and Subtitle A STUDY OF THE EFFECT OF RADICAL LOAD DISTRIBUTIONS ON CALIBRATED STRAIN GAGE LOAD EQUATIONS | | | | 5. Report Date July 1977 | |
| | | | | 6. Performing Organization Code | |
| 7. Author(s) Jerald M. Jenkins and Albert E. Kuhl | | | | 8. Performing Organization Report No. H-984 | |
| 9. Performing Organization Name and Address Dryden Flight Research Center P. O. Box 273 Edwards, California 93523 | | | | 10. Work Unit No. 505-02-23 | |
| | | | | 11. Contract Grant No. | |
| 12. Sponsoring Agency Name and Address National Aeronautics and Space Administration Washington, D.C. 20546 | | | | 13. Type of Report and Period Covered Technical Memorandum | |
| | | | | 14. Sponsoring Agency Code | |
| 15. Supplementary Notes | | | | | |
| 16. Abstract <p>For several decades, calibrated strain gages have been used to measure loads on airplanes. The accuracy of the equations used to relate the strain gage measurements to the applied loads has been based primarily on the results of the load calibration. This paper presents an approach for studying the effect of widely varying load distributions on strain gage load equations. The computational procedure presented provides a link between the load calibration and the load to be measured in flight.</p> <p>A matrix approach to equation selection is presented. This matrix approach, which is based on equation standard error, load distribution, and influence coefficient plots of the strain gage equations, is applied to a complex, delta-wing structure.</p> | | | | | |
| 17. Key Words (Suggested by Author(s)) Strain gages Loads Load equations | | | 18. Distribution Statement Unclassified - Unlimited Category: 39 | | |
| 19. Security Classif. (of this report) Unclassified | | 20. Security Classif. (of this page) Unclassified | | 21. No. of Pages 34 | |
| 22. Price* | | | | | |

*For sale by the National Technical Information Service, Springfield, Virginia 22161

A STUDY OF THE EFFECT OF RADICAL LOAD DISTRIBUTIONS ON CALIBRATED STRAIN GAGE LOAD EQUATIONS

Jerald M. Jenkins and Albert E. Kuhl
Dryden Flight Research Center

INTRODUCTION

For several decades, airplane flight loads have been measured using calibrated strain gages. The basic approach, which was formally documented in 1954 (ref. 1), consists of two distinct processes. First the information from a point load calibration of the lifting surface is used to obtain a linear expression that relates the applied loads to the strain gage outputs. The second process is the acquisition of flight data, which involves deducing flight loads from flight-measured strains. The empirical relationships established during the ground load calibration are used in the deductive process.

The procedure to evaluate the validity of a load equation has been a restricted one. It consists of obtaining a set of calculated loads from the equation based on the strain information obtained from each of the applied calibration loads. In other words, the accuracy of the equation is assessed only on the basis of information developed during the load calibration. In general, the distributions and magnitudes of the flight loads to be measured are not considered. Therefore, the range of applicability of the equation is not established.

These conventional procedures have, in great part, served the needs of flight test and research programs. However, with the evolution of supersonic and hypersonic airplanes, the measurement of flight loads has become more complex. In particular, many problems have resulted from low aspect ratio fins (ref. 2) and delta-wing airplanes (refs. 3 to 5). Little additional work has been done to assess the applicability of conventional processes to recently developed aircraft. In many recent studies, the point load calibration has been replaced by distributed and semidistributed load calibrations. The introduction of such approaches provides reason to question the validity of the conventional processes for evaluating the accuracy and applicability of a load equation.

This report uses a computational procedure to examine the validity and applicability of various load equations for various load distributions. The computational procedure used is designed to link the ground load calibration to the measurement to be made in flight.

SYMBOLS

| | |
|----------------|--|
| B | bending moment |
| I_{ji} | influence coefficient for the j th strain gage due to a load applied at the i th load point, μ_{c_j}/L_{c_i} , 1/N (1/lb) |
| i | discrete load point |
| j | discrete strain gage |
| L_{c_i} | calibration load applied at the i th load point, N (lb) |
| L_{l_i} | local load applied at the i th load point, N (lb) |
| L_T | total load applied to the wing, N (lb) |
| S | shear load |
| T | torsion load |
| δ | voltage change resulting from straining the active arms of a strain gage bridge |
| δ_{cal} | reference voltage change resulting from shunting a calibrated resistor across one arm of a strain gage bridge |
| μ | nondimensional strain gage response, δ/δ_{cal} |
| μ_{c_j} | nondimensional strain gage response for the j th strain gage due to the applied calibration load |
| μ_{T_j} | summation of total nondimensional strain gage responses for the j th strain gage due to the total superposition of all local loads |
| $\mu_{t_{ji}}$ | total nondimensional strain gage response for the j th strain gage due to the local loading at the i th load point |
| Subscripts: | |
| m | total number of strain gages on wing |
| n | total number of calibration load points on wing |

DELTA-WING TEST STRUCTURE

The structural skeleton of a complex delta-wing aircraft is shown in figure 1. The wing, which is of a multispar construction with an outboard engine nacelle, was thoroughly instrumented with strain gages and a load calibration was performed (refs. 3 to 5). The locations of the strain gages are shown in figure 2. Even-numbered strain gages are configured to sense shearing strains and odd-numbered gages are configured to sense bending strains. The completeness of the strain gage instrumentation and the load calibration of the structure provide the basis for the analytical study contained in this paper.

LOAD EQUATIONS

Load equations that relate applied wing loads to wing root strain gages are presented in table 1. These equations were derived by the method described in reference 4 and the equation numbers are consistent with those given in that reference. Additional discussion of the equations is presented in reference 6. The letter S, B, or T in an equation number indicates whether the equation was developed for shear, bending moment, or torsion, respectively. The three digit subscript, such as 302, identifies the strain gage associated with the output, μ . All the shear and torsion equations use five strain gage outputs; the bending moment equations require the outputs of only two or three strain gages.

The procedure for the error analysis of these equations is discussed in references 1 and 4. The standard error of each equation is given in table 2.

COMPUTATIONAL PROCEDURES

The conventional processes used to acquire flight loads data are listed in table 3. The laboratory process includes the activities that result from applying loads to a lifting surface, measuring the strain gage responses, and deriving a mathematical relationship between the loads and the responses. The flight testing includes the acquisition of the flight test data and the use of the laboratory data to interpret the information. In the past, this process has been a closed-loop situation. Accuracy statements have been based on the laboratory calculations and estimates of the flight data recording system capabilities.

A more complete knowledge of the applicability of an equation developed from laboratory and flight test processes can be acquired by computational means. Two types of computational processes are outlined in table 3. The first computational procedure is reported in reference 6. This computation uses a finite element structural model to determine where strain gages should be located and how they should be combined into equations before the load calibration is done. The second computation evaluates the ability of a particular equation to calculate widely varying

distributions of load. The study of this computation and its results is the basis for this paper.

The distribution of aerodynamic loads on a lifting surface, such as an airplane wing, varies in both the chord and span directions, depending on flow conditions and the attitude of the lifting surface. The most dramatic variations occur in the chord direction. The variations for three characteristic loadings are shown in figure 3. Two of the three loadings (figs. 3(a) and 3(b)) can be attributed to variations in Mach number. The forward center of pressure loading is developed from the classic subsonic chordwise pressure distribution of reference 7 and the spanwise distribution of subsonic pressure developed in reference 8. The central center of pressure loading is typical of supersonic flow where the load is distributed uniformly over the lifting surface. The third distribution (fig. 3(c)), which represents a center of pressure located near the trailing edge of the lifting surface, typically results from control surface-induced loads, which are defined in reference 9. These three loadings represent a widely varying set for computational analysis.

A schematic of the computational procedure is shown in figure 4. The laboratory load calibration provides information from which experimentally determined influence coefficients are obtained and load equations are developed. These coefficients and equations are the keys to the computation. Each of the hypothetical loadings can be divided into local area loadings. The manner in which the loading is subdivided is based on the location of laboratory calibration loads. For the present study, the wing surface was subdivided to correspond to the calibration load point locations, as shown in figure 5.

A typical local loading is shown in figure 6. This local loading can be used to calculate the total strain gage output for the j th strain gage and the i th load point, $\mu_{t_{ji}}$, which can be determined from the equation

$$\mu_{t_{ji}} = (L_{l_i})(I_{ji})$$

where L_{l_i} is the local loading at the i th point and I_{ji} is the influence coefficient determined from the load calibration. The influence coefficient is defined as

$$I_{ji} = \frac{\mu_{c_j}}{L_{c_i}}$$

where μ_{c_j} is the total output of the j th strain gage due to the calibration load, L_{c_i} , applied at the i th load point.

The total outputs for all the strain gages can be calculated for all the local loadings. Hence, for any discrete strain gage, j , the total output, μ_{T_j} , due to the total load, L_T , can be expressed as

$$\mu_{T_j} = \sum_{i=1}^{i=n} (L_{l_i})(I_{ji})$$

where n is the total number of local loadings. The number n also corresponds to the number of load points used in the laboratory load calibration.

The total output μ_{T_j} is input directly to a load equation that was developed using the j th strain gage. If m strain gages are available, then for each way the load is distributed, the outputs to be calculated are $\mu_{T_1}, \mu_{T_2}, \dots, \mu_{T_j}, \dots, \mu_{T_m}$. For this study, the load was distributed in the three ways shown in figure 3. Therefore, there are three identical total loads, L_T , which are distributed in three ways by way of the local loadings, L_{l_i} . From this information, local strain gage outputs, $\mu_{t_{ji}}$, can be calculated. Then total strain outputs, μ_{T_j} , can be calculated for m strain gages for each of the three total load distributions. Three known load distributions can now be applied mathematically to the structure; then these loads can be calculated based on the experimental influence coefficients and the total superimposed strain outputs. If the equations are universally applicable, the calculated load should approximate the applied load, L_T . If for one or more of the three load distributions a particular equation fails to calculate L_T with suitable accuracy, the equation should be rejected because it is not universally applicable to all load distributions.

INFLUENCE COEFFICIENT PLOTS

Probably the most informative manner of presentation for load calibration data is the influence coefficient plot. The influence coefficient plot provides a way to look at the output per unit applied load as a function of span location for a given chord location for each strain gage bridge (ref. 6). A plot of this nature is useful in determining whether a bridge is affected predominately by shear, bending moment, or torsion loads, by a combination of two, or even by all three. This is illustrated in figure 7. The ideal responses are those from strain gages that are sensitive only to shear, bending moment, or torsion loads. Ideal responses are rare. More commonly, the influence coefficient plot shows the combined effects of shear, bending moment, and torsion loads. This type of response, which is referred to herein as a complex response, is frequently nonlinear in nature (ref. 6). The

purpose of combining several strain gages into an equation is to attempt to create an ideal or nearly ideal response.

An equation can be plotted similarly and examined on the same basis. This provides an excellent way to examine the characteristics of the equations in terms of the load location. Influence coefficient plots for the equations presented in table 1 are shown in figures 8, 9, and 10. The shear equations are plotted in figure 8, the bending moment equations in figure 9, and the torsion equations in figure 10. In the ideal case, these plots would be similar to the shear, bending moment, and torsion plots in figure 7(a). An ideal shear equation would appear as a horizontal straight line. An ideal bending moment equation would appear as a straight line passing through the origin. An influence coefficient plot of an ideal torsion equation would have the same shape as the planform of the constant chord lines.

RESULTS AND DISCUSSION

The computational procedure shown in figure 4 was applied to the load-calibrated wing, the derived equations, and the set of hypothetical loads discussed in previous sections. A 44,480-newton (10,000-pound) load was applied mathematically to the wing structure using the three distributions shown in figure 3. These load distributions are referred to hereafter as the forward center of pressure loading, the central center of pressure loading, and the aft center of pressure loading. The procedures outlined in the Computational Procedures section were used to apply the local loadings and to calculate the total output for each of the strain gages under each load condition. The outputs for each of the three load distributions were input to the appropriate equations from table 1 and the resulting calculated loads for shear, bending moment, and torsion were then compared to the known applied load. The results are shown in figures 11 to 13.

Shear Loads

In figure 11, the calculated shear loads are compared to the 44,480-newton (10,000-pound) applied load for the eight shear equations. The figure shows that the calculated loads are smaller than the mathematically applied load. In addition, the calculated loads more closely approximate the mathematically applied load for the forward and central center of pressure loadings than for the aft center of pressure loading. There is a significant variation in calculated load from equation to equation for all three load distributions. The variation is as high as 20 percent.

Figure 11 also shows that equation 93S comes closer to calculating the three mathematically applied loads than any of the other equations. However, table 2 shows that equation 93S has the second highest standard error of the eight shear equations. Equation 95S is almost as good as equation 93S for calculating the applied load and has a significantly lower standard error. The influence coefficient plots of equations 93S and 95S (fig. 8) show that the chord lines for equation 95S are more closely packed and more closely resemble straight lines.

Equations 91S and 92S appear to be the least favorable shear equations based on the calculative test used in this paper. The influence coefficient plot for equation 91S shows a lot of scatter and some significant nonlinearities. The influence coefficient plot for equation 92S, however, does not look as bad as the results of the calculative test imply. Comparison of the standard errors of the equations and examination of the influence coefficient plots of the equations do not reveal any obvious clue as to why equations 93S and 95S result in calculated shear loads closer to the analytically applied shear load than those calculated with equations 91S and 92S. However, since all eight shear equations use logical combinations of strain gages, little variation would be expected. If these equations were contrasted with equations having illogical strain gage combinations, trends would probably be more evident.

The landing gear wheel well is between the spars on which strain gage bridges 306/307 and 308/309 are located. This wheel well represents an interruption in the continuity of the structure. It is worth noting that equations 91S and 92S have three strain gages forward of the wheel well and two strain gages aft of the wheel well, whereas equations 93S and 95S have two strain gages aft of the wheel well and three forward of the wheel well. Further investigation would be necessary to determine whether this difference is significant.

Two other factors of importance in a study of this nature are the magnitude of the calibration loads and how the loads are distributed over the surface of the wing. Figure 14 shows the relative magnitudes of the calibration loads for this study. The lengths of the vectors represent the relative magnitudes of the loads. As is true in the calibration of most aircraft wings, the distribution of the calibration loads does not correspond to the probable distribution of the flight loads. The largest calibration loads were applied along an inboard chord from near the leading edge to near the trailing edge; the outboard leading edge and the entire trailing edge were subjected to very small calibration loads. In flight, large loads are likely to occur near the trailing edge where the control surfaces are located and near the leading edge due to the basic character of chordwise subsonic pressure distributions. The small calibration loads on the trailing edge probably contribute greatly to the largest discrepancy seen in figure 11, which is the discrepancy between the calculated and mathematically applied shear loads for the aft center of pressure loading.

The local loadings that can be applied to a wing structure depend on the bearing strength available at the particular location; therefore, the calibration loads are generally sized according to the local strength. This was the case for this wing. Figures 11 and 14 indicate that the calibration may be inadequate for deriving equations suitable for describing loadings in an extreme aft position.

Bending Moments

The comparison of calculated and mathematically applied bending moments is presented in figure 12. The variation in the magnitude of the bending load is caused by the variation in the distribution of the 44,480-newton (10,000-pound) load. As in the comparison for shear loads, the calculated bending moments are smaller than the mathematically applied bending moments. In general, the calculated and

mathematically applied values for the bending moments correlate better than those for the shear loads. For the forward and aft center of pressure loadings, the calculated bending moments for all the equations examined are within 4 percent of the mathematically applied bending moments. The correlation is poorer for the central center of pressure loading: The calculated bending moments are 5 to 10 percent lower than the mathematically applied bending moments. The variation of the calculated bending moments among the equations is quite small for each of the load distributions.

In the influence coefficient plots for the bending moment equations (fig. 9), no equation appears to be superior to the others. Equation 81B is the least linear and has the highest standard error of the four equations; therefore, it could be considered to be the least reliable of the group. However, equations 80B, 82B, and 83B have no distinguishing features that allow further ranking. Equation 80B uses only two strain gage bridges; hence, it might be chosen because it would require fewer data recording channels. As in the case of the shear equations, there would be more contrast if the gage selection included illogical choices.

Torsion Loads

Torsion loads have historically been the most difficult loads to measure on low aspect ratio and delta-wing lifting surfaces. The wing studied in this paper is no exception. In addition, caution must be exercised when examining torsion data because the quantities are dependent on the location of the reference axis. For this study, the reference axis is at fuselage station 970 (ref. 4), which is at approximately 25 percent of the mean aerodynamic chord of the wing panel.

The comparison of the calculated and mathematically applied torsion loads is presented in figure 13. The magnitude of the mathematically applied torsion loads varies depending on the distribution of the 44,480-newton (10,000-pound) load. The figure shows that the calculated torsion loads for the forward center of pressure loading exceed the mathematically applied torsion load by 4520 newton-meters (40,000 inch-pounds) to 12,430 newton-meters (110,000 inch-pounds). The variation of the calculated torsion load among the equations is as much as 7910 newton-meters (70,000 inch-pounds). The calculated torsion loads for the central center of pressure loading are smaller than the mathematically applied torsion loads by 7910 newton-meters (70,000 inch-pounds) to 16,950 newton-meters (150,000 inch-pounds). The variation of the calculated torsion load among the equations is as large as 9040 newton-meters (80,000 inch-pounds). The calculated torsion loads for the aft center of pressure loading show the largest deviations from the mathematically applied load: The calculated torsion loads are smaller by 56,500 newton-meters (500,000 inch-pounds) to 84,750 newton-meters (750,000 inch-pounds). The variation of the calculated torsion loads among the equations was as large as 28,250 newton-meters (250,000 inch-pounds).

The standard errors of the six torsion equations (table 2) range from 2585 newton-meters (22,880 inch-pounds) to 4740 newton-meters (41,920 inch-pounds). For the forward center of pressure loading, the calculated torsion loads from equations 90T and 91T have the largest and smallest deviations from the

mathematically applied loads. However, these two equations also have the largest standard errors of the six equations. The deviations of the calculated torsion loads from the mathematically applied torsion loads for the central center of pressure loading are clearly outside the ranges of the standard errors for the torsion equations. For the aft center of pressure loading, the deviations are at least an order of magnitude larger than the standard errors for this set of torsion equations. This discrepancy between the calculated and mathematically applied torsion loads for the aft center of pressure loading corresponds to the discrepancy for the shear loads and is assumed to be influenced by the low magnitude of the calibration loads at the trailing edge (fig. 14). It is also important to note that the deviation of the calculated torsion load from the mathematically applied torsion load increased as the center of pressure of the loading became more remote from the reference axis.

Equation 84T has the lowest standard error of the torsion equations. Based on the mathematical computation, equations 91T, 85T, and 90T best measure the loadings for the forward, central, and aft centers of pressure, respectively. The influence coefficient plots indicate that equations 84T, 85T, and 88T are equally the best of the torsion equations.

Equation Selection Matrices

Thus far, the standard errors of the equations, the mathematical computation using the three load distributions, and the influence coefficient plots of the equations have been used individually to evaluate whether an equation can calculate loads accurately. In table 4, these factors are presented collectively in matrix form for all the equations. Each equation was evaluated on the basis of five criteria: the standard error, the accuracy of the calculated loads for the forward loadings, the accuracy of the calculated loads for the central loadings, the accuracy of the calculated loads for the aft loadings, and the appearance of the influence coefficient plot. The equations were ranked on the basis of each of the five criteria and an X was recorded in the matrix for each equation that ranked in the top 50 percent of the group for a given criterion. When distinguishing factors were not clear or did not divide the group of equations into two halves, more or less than 50 percent of the equations were marked for that criterion. This simple approach provides a general identification of the most desirable equations based on the five criteria selected. There are, of course, many other methods and criteria by which a similar matrix can be established.

The value of such a matrix approach is clear. The discussion of the equations based on individual criteria gives no definite answer as to which equation to use. In addition, no equation recurs as the best for all or even most criteria. The matrix approach combines the accumulated information to give a concise overview. The matrices in table 4 show that equations 95S, 92S, and 93S are the most desirable for calculating shear loads; equations 82B and 83B are the most desirable for calculating bending loads; and equations 85T and 88T are the most desirable for calculating torsion loads.

CONCLUDING REMARKS

The task of obtaining reliable strain gage load equations is still complex, even after several decades of experience. Various criteria can be used for evaluating load equations. Statistical calculations such as standard errors provide no link to the load to be measured in flight. Influence coefficients are helpful in equation selection; however, interpretation is very difficult, particularly for the novice. The mathematical computation introduced in this paper provides a means of examining the behavior of equations for radically varying distributions of load. The use of a load-distributing computational procedure to augment the error calculations and influence coefficient plots developed from the load calibration is of great value in that it links the load calibration to the flight load to be measured rather than just to the calibration load. This aspect cannot be overlooked if a system of equations is to be objectively evaluated for universal application.

A matrix approach to equation selection is presented and an example is given. The results show that the best equations can be selected from a group by using a set of criteria from which a matrix can be established. The five criteria selected for use in the example in this paper are not necessarily recommended as a universal set of criteria. However, it is strongly recommended that a matrix approach be used for equation selection. In addition, it is recommended that the matrix criteria include factors that extend beyond the information of the load calibration and, hopefully, link the load calibration to the flight load to be measured.

*Dryden Flight Research Center
National Aeronautics and Space Administration
Edwards, Calif., March 22, 1977*

REFERENCES

1. Skopinski, T. H.; Aiken, William S., Jr.; and Huston, Wilber B.: Calibration of Strain-Gage Installations in Aircraft Structures for the Measurement of Flight Loads. NACA Rept. 1178, 1954.
2. Jenkins, Jerald M.; Tang, Ming H.; and Pearson, George P. E.: Vertical-Tail Loads and Control-Surface Hinge-Moment Measurements on the M2-F2 Lifting Body During Initial Subsonic Flight Tests. NASA TM X-1712, 1968.
3. Jenkins, Jerald M.: An Introduction to Thermal Effects in Strain Gage Load Measurement. NASA YF-12 Flight Loads Program, NASA TM X-3061, 1974, pp. 1-27.
4. Sefic, Walter J.; and Reardon, Lawrence F.: Loads Calibration of the Airplane. NASA YF-12 Flight Loads Program, NASA TM X-3061, 1974, pp. 61-107.
5. Jenkins, Jerald M.; and Kuhl, Albert E.: Summary of Recent Results Pertaining to Strain Gage Load Measurement Technology on High Speed Aircraft. NASA YF-12 Flight Loads Program, NASA TM X-3061, 1974, pp. 303-323.
6. Jenkins, Jerald M.; Kuhl, Albert E.; and Carter, Alan L.: The Use of a Simplified Structural Model as an Aid in the Strain Gage Calibration of a Complex Wing. NASA TM X-56046, 1977.
7. Allen, H. Julian: General Theory of Airfoil Sections Having Arbitrary Shape or Pressure Distribution. NACA Rept. 833, 1945.
8. DeYoung, John; and Harper, Charles W.: Theoretical Symmetric Span Loading at Subsonic Speeds for Wings Having Arbitrary Plan Form. NACA Rept. 921, 1948.
9. Tucker, Warren A.; and Nelson, Robert L.: Theoretical Characteristics in Supersonic Flow of Two Types of Control Surfaces on Triangular Wings. NACA Rept. 939, 1949.

TABLE 1. —LOAD EQUATIONS

| Equation number | Load equation |
|-----------------|---|
| 87S | $S = -6824(\mu)_{302} - 8553(\mu)_{306} - 11,442(\mu)_{310} - 6124(\mu)_{318} - 5036(\mu)_{311}$ |
| 88S | $S = -6599(\mu)_{302} - 8498(\mu)_{306} - 6380(\mu)_{307} - 13,389(\mu)_{312} - 4562(\mu)_{320}$ |
| 89S | $S = -4943(\mu)_{300} - 10,725(\mu)_{306} - 5825(\mu)_{305} - 12,713(\mu)_{312} - 5436(\mu)_{320}$ |
| 91S | $S = -5496(\mu)_{300} - 14,175(\mu)_{306} - 13,352(\mu)_{312} - 3914(\mu)_{320} - 1509(\mu)_{311}$ |
| 92S | $S = -6349(\mu)_{302} - 6500(\mu)_{306} - 7632(\mu)_{308} - 9083(\mu)_{318} - 10,715(\mu)_{311}$ |
| 93S | $S = -5305(\mu)_{302} - 6669(\mu)_{304} - 10,817(\mu)_{307} - 13,557(\mu)_{312} - 5086(\mu)_{320}$ |
| 94S | $S = -5960(\mu)_{302} - 6703(\mu)_{306} - 7716(\mu)_{305} - 13,104(\mu)_{314} - 1809(\mu)_{320}$ |
| 95S | $S = -5535(\mu)_{302} - 6501(\mu)_{306} - 9014(\mu)_{305} - 13,578(\mu)_{312} - 5600(\mu)_{322}$ |
| 80B | $B = -1,553,600(\mu)_{313} - 839,389(\mu)_{305}$ |
| 81B | $B = -2,022,520(\mu)_{311} - 481,782(\mu)_{303}$ |
| 82B | $B = -550,814(\mu)_{309} - 716,907(\mu)_{305} - 1,326,970(\mu)_{313}$ |
| 83B | $B = -742,032(\mu)_{317} - 859,973(\mu)_{303} - 1,117,860(\mu)_{311}$ |
| 84T | $T = -669,400(\mu)_{302} - 1,479,900(\mu)_{303} + 628,278(\mu)_{316} + 280,942(\mu)_{320} + 1,331,200(\mu)_{324}$ |
| 85T | $T = -893,000(\mu)_{302} - 979,300(\mu)_{305} + 591,072(\mu)_{314} + 573,000(\mu)_{320} + 1,480,600(\mu)_{324}$ |
| 88T | $T = -656,100(\mu)_{302} - 1,492,900(\mu)_{303} + 588,600(\mu)_{314} + 580,000(\mu)_{320} + 1,330,900(\mu)_{324}$ |
| 89T | $T = -327,000(\mu)_{302} - 2,513,900(\mu)_{303} + 487,700(\mu)_{316} + 949,442(\mu)_{322} + 954,616(\mu)_{311}$ |
| 90T | $T = -284,000(\mu)_{300} - 2,569,500(\mu)_{303} + 852,000(\mu)_{318} + 956,400(\mu)_{324} + 905,300(\mu)_{311}$ |
| 91T | $T = -582,600(\mu)_{300} - 2,342,900(\mu)_{305} + 440,687(\mu)_{314} + 1,051,570(\mu)_{322} + 1,551,130(\mu)_{311}$ |

TABLE 2.—STANDARD ERRORS OF LOAD EQUATIONS

(a) Shear equations

| Equation | Equation standard error, N (lb) |
|----------|------------------------------------|
| 87S | 1176.9 (264.6) |
| 88S | 1557.7 (350.2) |
| 89S | 1404.7 (315.8) |
| 91S | 1744.9 (392.3) |
| 92S | 1355.3 (304.7) |
| 93S | 1958.9 (440.4) |
| 94S | 2610.5 (586.9) |
| 95S | 1408.2 (316.6) |

(b) Bending moment equations

| Equation | Equation standard error, N-m (in-lb) |
|----------|---|
| 80B | 2661 (23,552) |
| 81B | 3693 (32,681) |
| 82B | 2555 (22,616) |
| 83B | 1439 (12,741) |

(c) Torque equations

| Equation | Equation standard error, N-m (in-lb) |
|----------|---|
| 84T | 2585 (22,875) |
| 85T | 3305 (29,251) |
| 88T | 3132 (27,719) |
| 89T | 3629 (32,116) |
| 90T | 4347 (38,471) |
| 91T | 4737 (41,922) |

TABLE 3. — BASIC PROCESSES OF STRAIN GAGE LOAD MEASUREMENT

| Laboratory (experimental) | Flight test | Computational | |
|--|---|--|---|
| | | Strain prediction | Load variation analysis |
| Apply known loads Measure strains Calculate influence coefficients Derive load equations Calculate applied loads Calculate errors | Experience forces Measure strains Apply load equations Calculate loads | Represent structure (model) Apply known loads analytically Calculate internal loads Calculate strains Calculate influence coefficients Compare with experimental data | Apply hypothetical loads Use experimental influence coefficients Apply load equations Calculate hypothetical loads Calculate errors |

TABLE 4.—EQUATION SELECTION MATRICES
[X identifies equations that give most favorable results]

(a) Shear equations

| Criteria | Equation | | | | | | | |
|----------------------------|----------|-----|-----|-----|-----|-----|-----|-----|
| | 87S | 88S | 89S | 91S | 92S | 93S | 94S | 95S |
| Standard error | X | --- | X | --- | X | --- | --- | X |
| Forward loading | --- | --- | --- | --- | X | X | X | X |
| Central loading | --- | --- | --- | --- | X | X | X | X |
| Aft loading | --- | X | --- | --- | --- | X | X | X |
| Influence coefficient plot | X | X | --- | --- | X | X | --- | X |

(b) Bending moment equations

| Criteria | Equation | | | |
|----------------------------|----------|-----|-----|-----|
| | 80B | 81B | 82B | 83B |
| Standard error | --- | --- | X | X |
| Forward loading | X | X | X | X |
| Central loading | --- | --- | X | X |
| Aft loading | X | --- | X | X |
| Influence coefficient plot | X | --- | X | X |

(c) Torsion equations

| Criteria | Equation | | | | | |
|----------------------------|----------|-----|-----|-----|-----|-----|
| | 84T | 85T | 88T | 89T | 90T | 91T |
| Standard error | X | X | X | --- | --- | --- |
| Forward loading | --- | X | X | --- | --- | X |
| Central loading | --- | X | X | --- | --- | X |
| Aft loading | --- | X | X | --- | X | --- |
| Influence coefficient plot | X | X | X | --- | --- | --- |

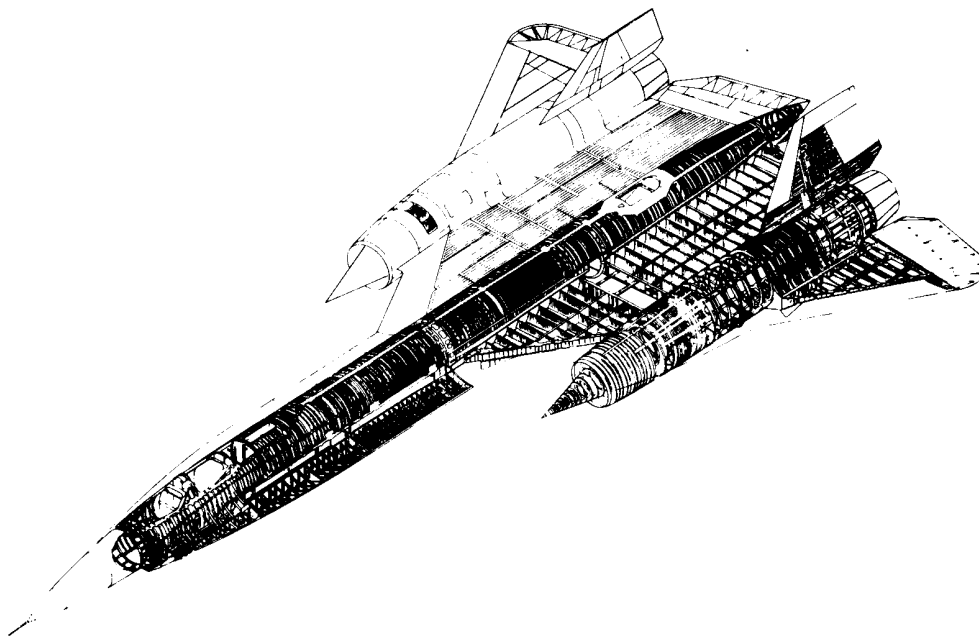


Figure 1. Structural skeleton of complex delta-wing aircraft.

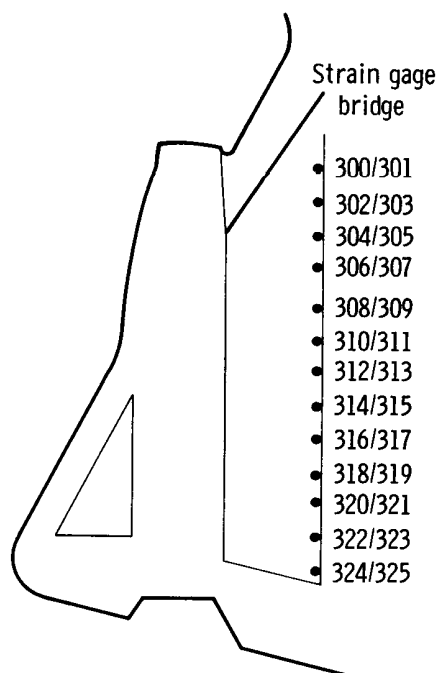
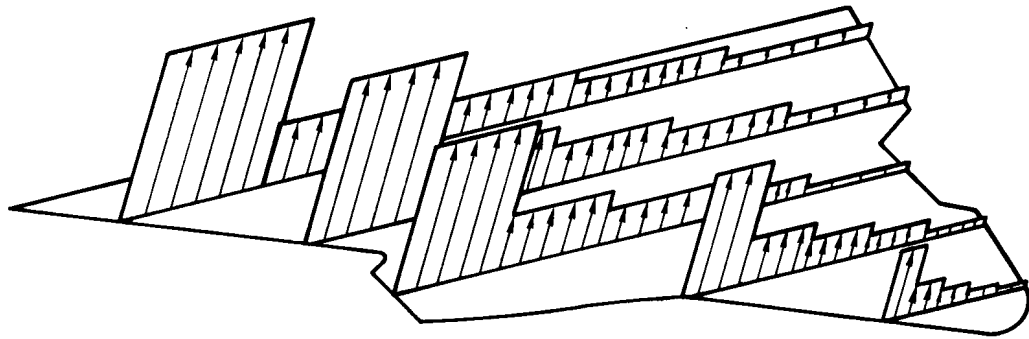
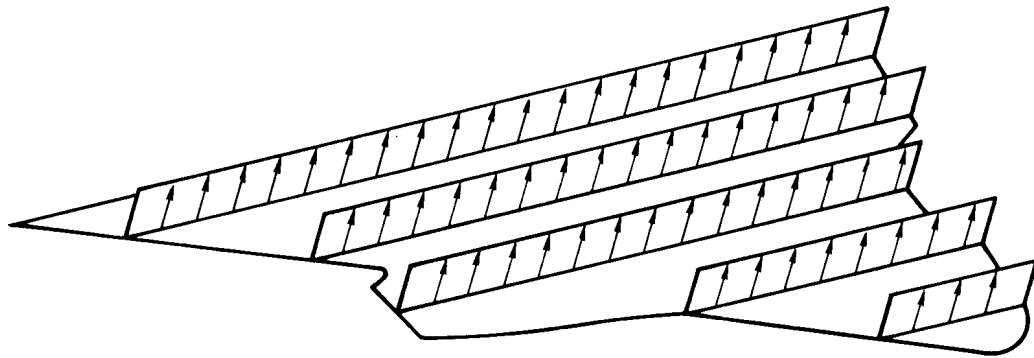


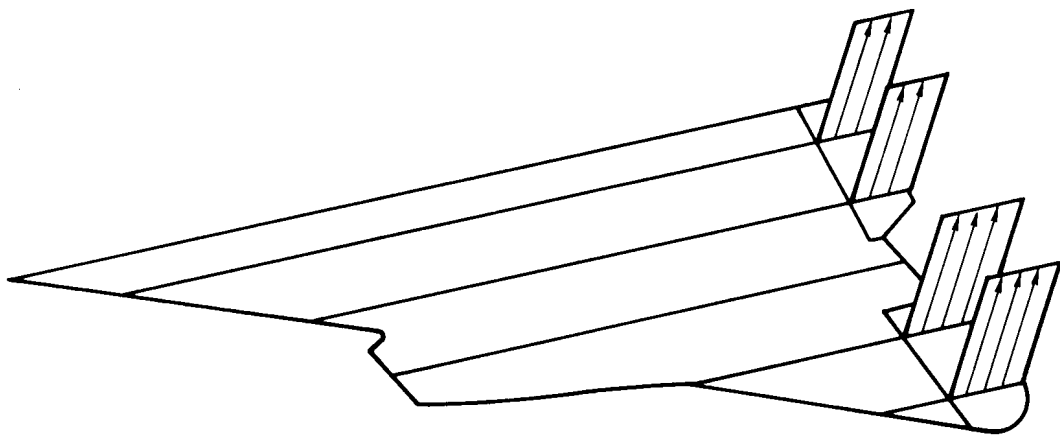
Figure 2. Location of strain gages with respect to wing planform.



(a) *Forward center of pressure.*



(b) *Central center of pressure.*



(c) *Aft center of pressure.*

Figure 3. Distribution of mathematically applied loads.

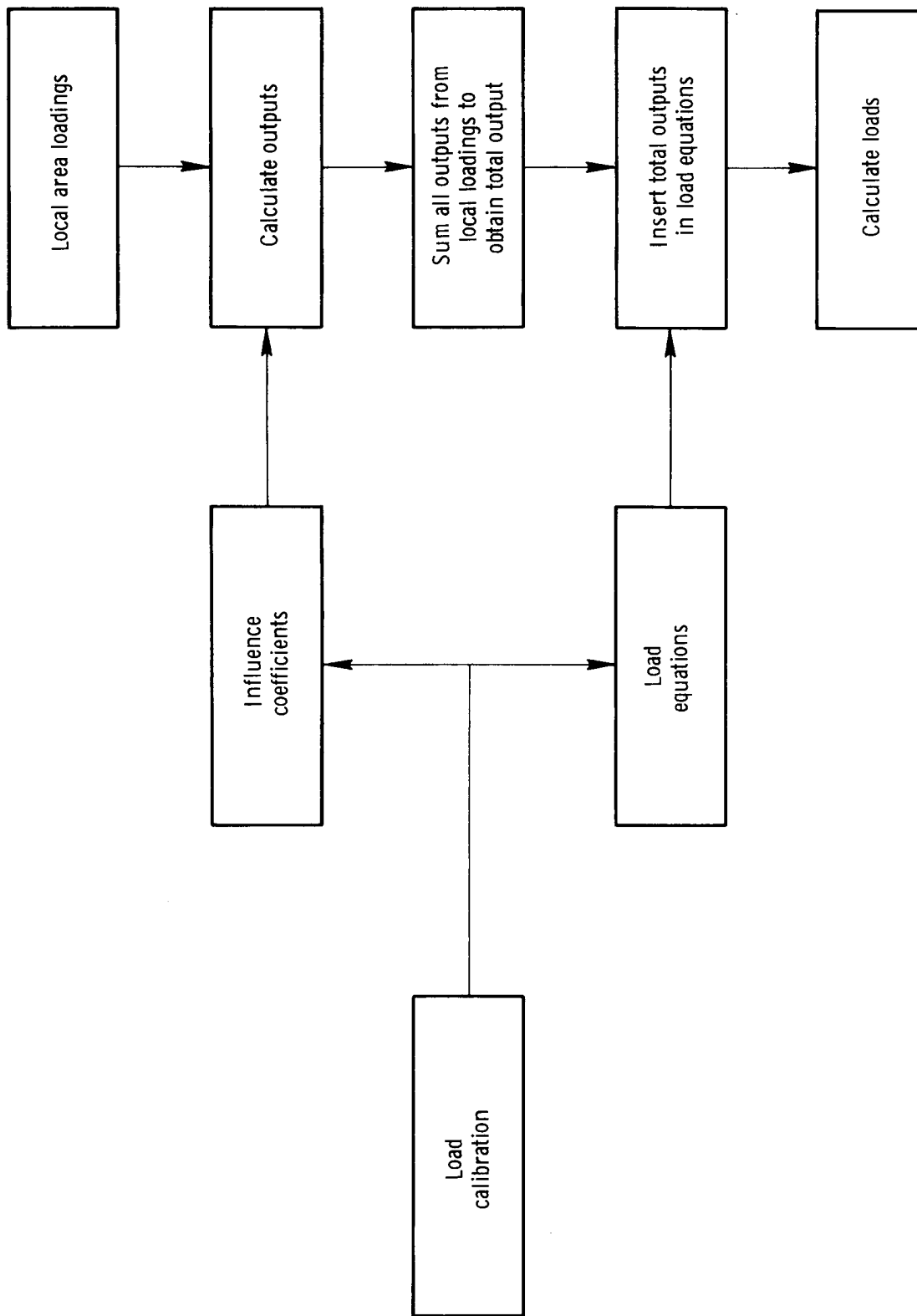


Figure 4. Schematic of computation of mathematically applied loads.

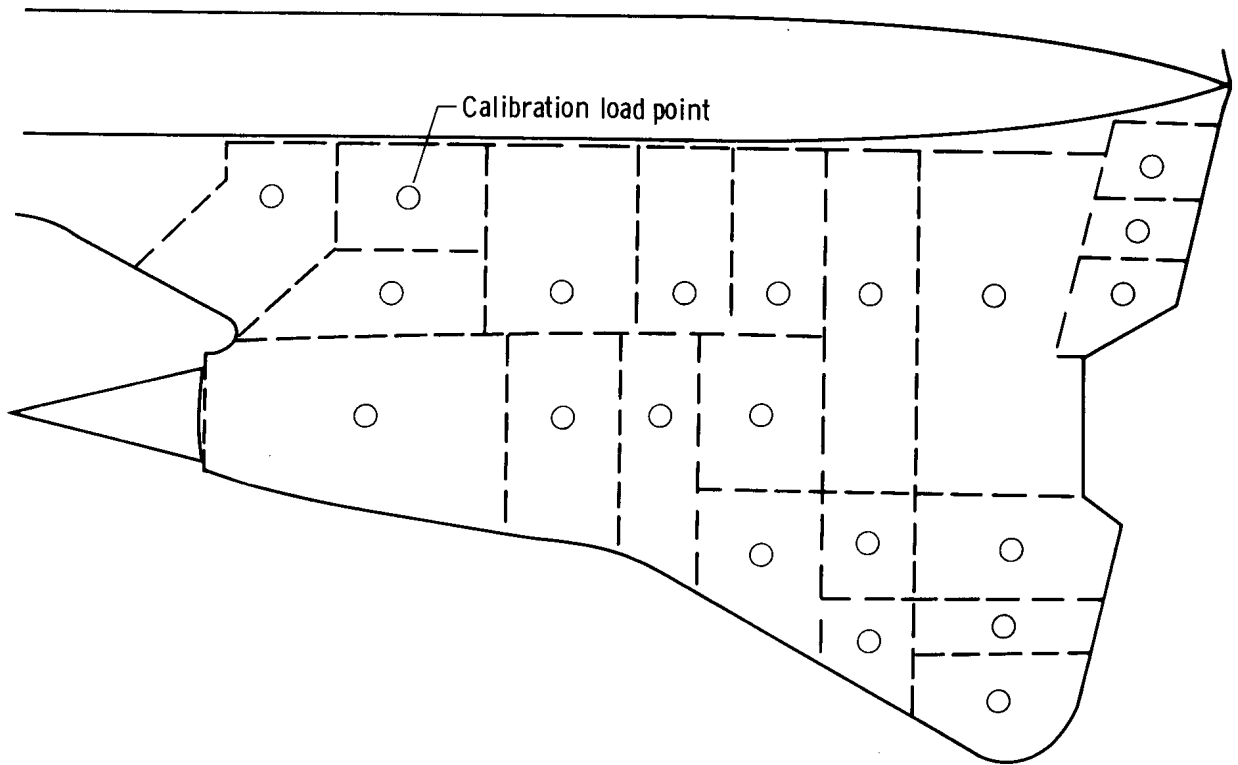


Figure 5. Subdivision of wing surface.

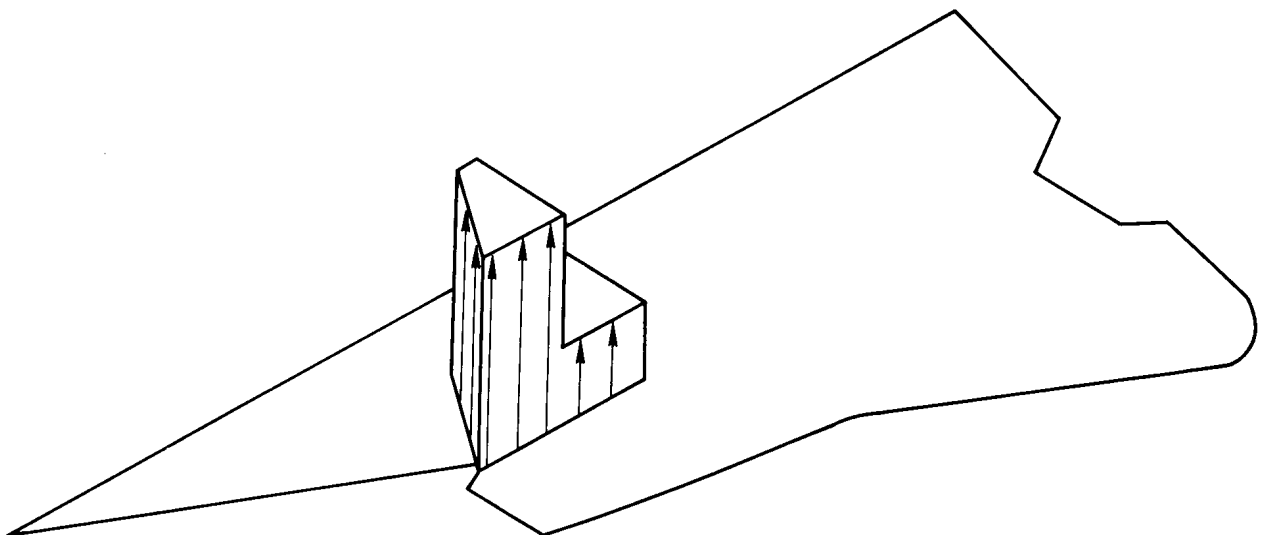
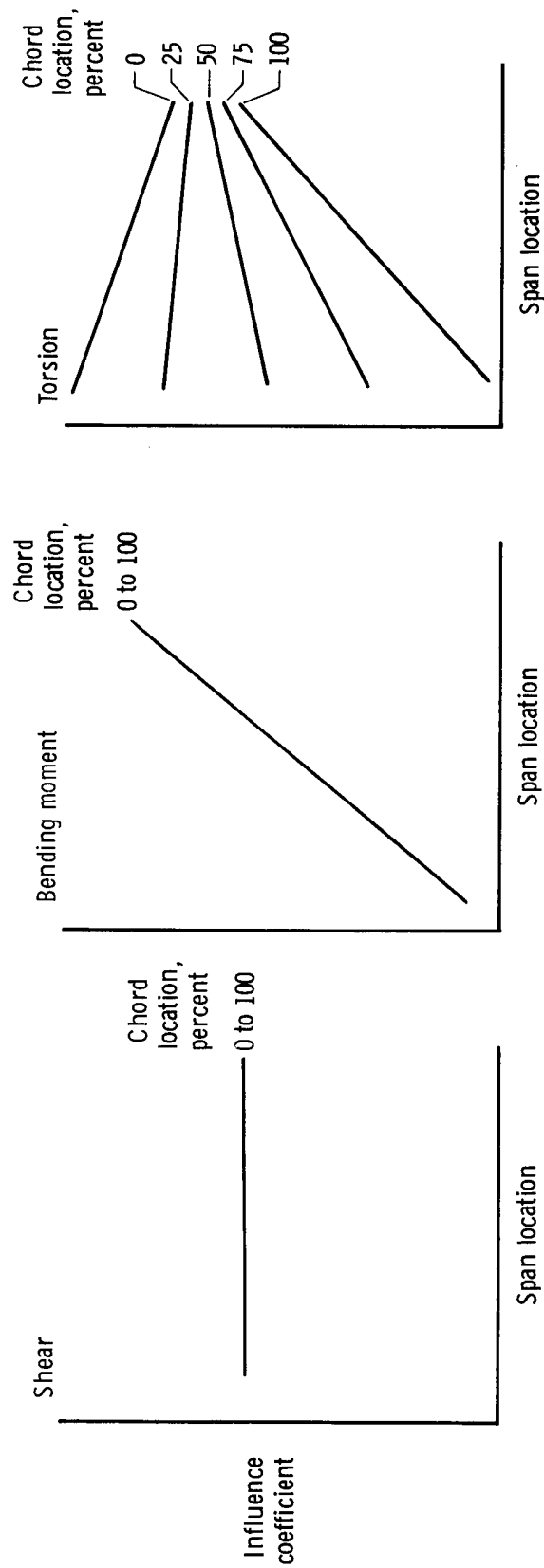
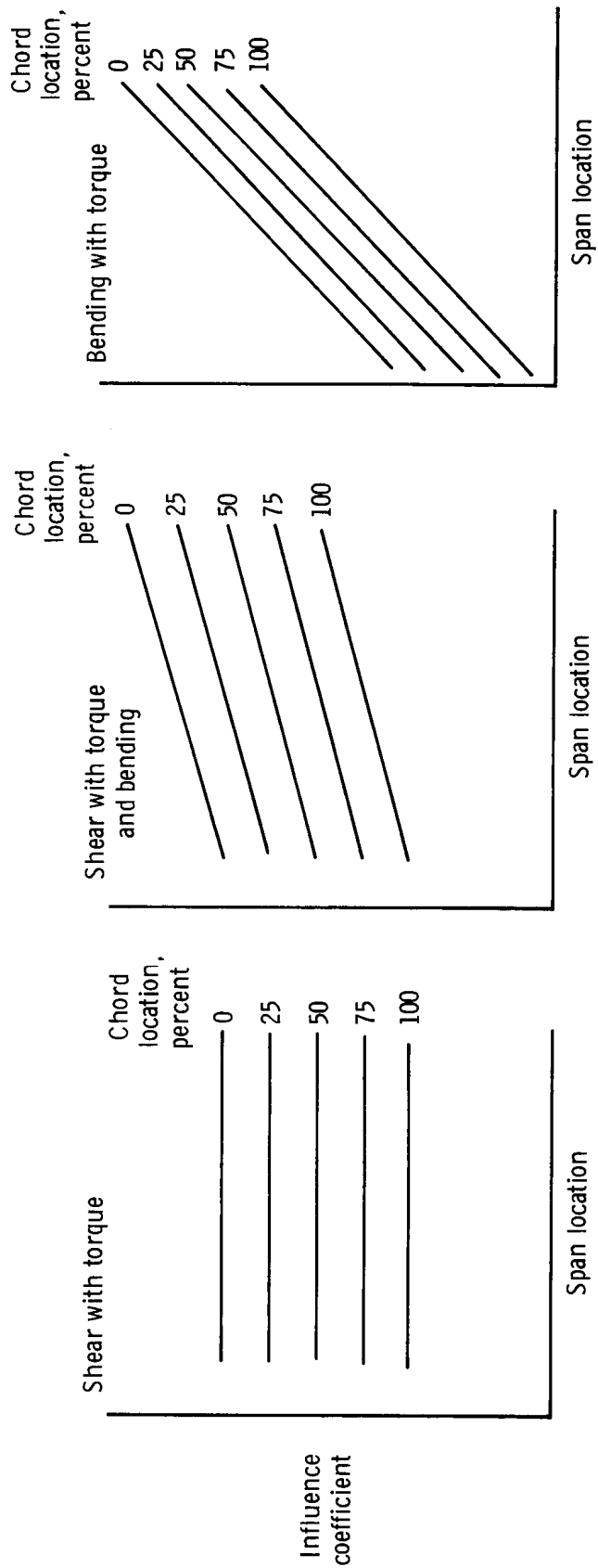


Figure 6. Typical local loading.



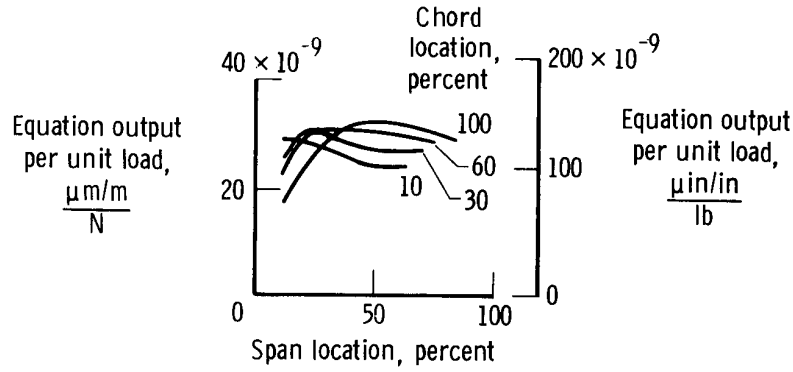
(a) Ideal responses.

Figure 7. Examples of strain gage influence coefficient plots.

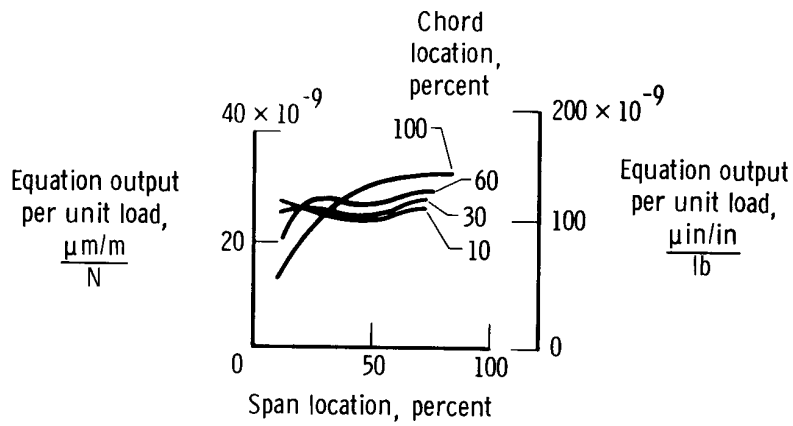


(b) Complex responses.

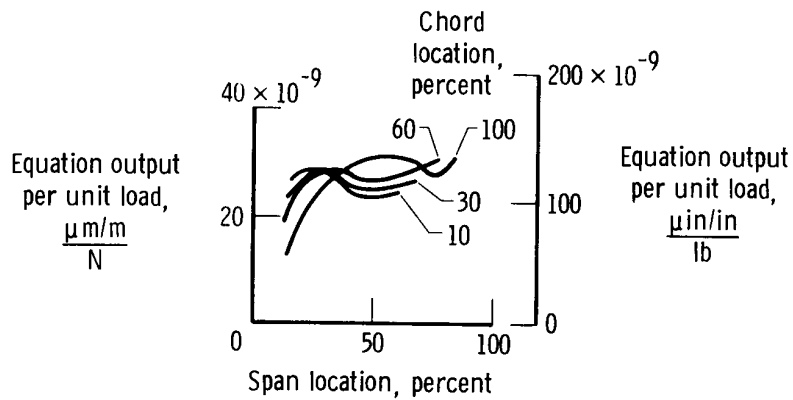
Figure 7. Concluded.



(a) Equation 87S.

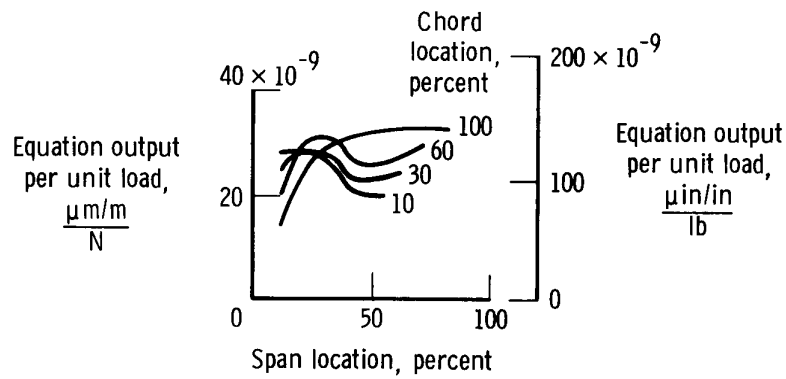


(b) Equation 88S.

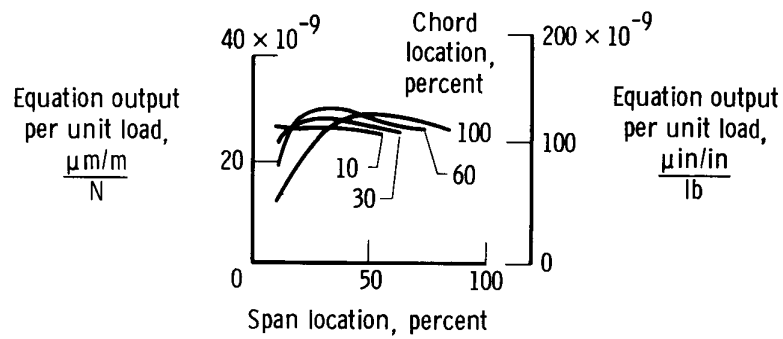


(c) Equation 89S.

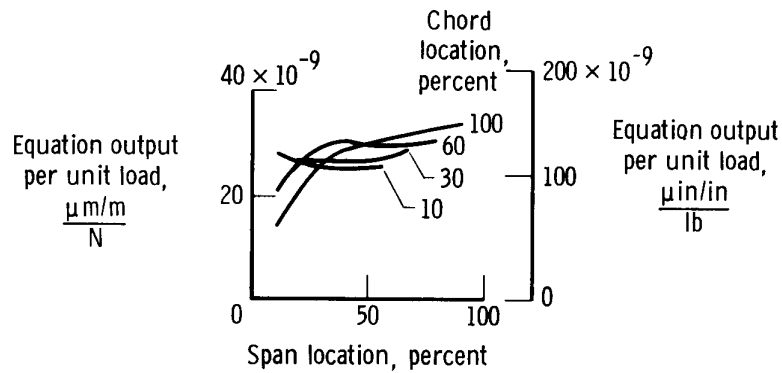
Figure 8. Influence coefficient plots of shear equations.



(d) Equation 91S.

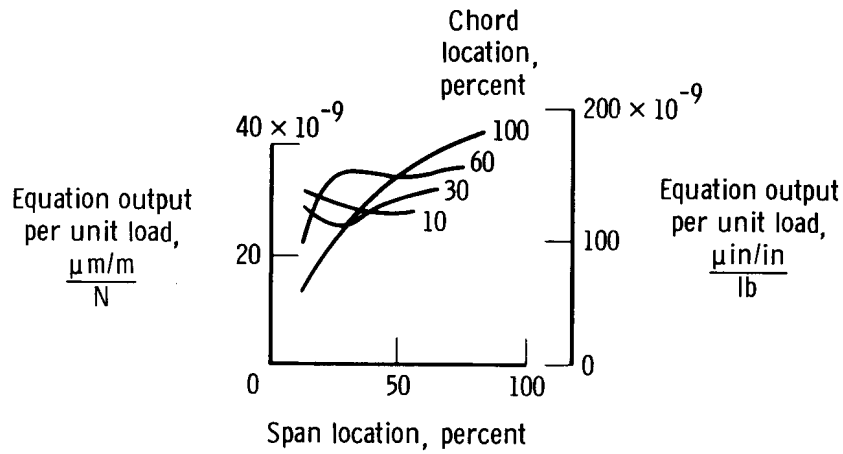


(e) Equation 92S.

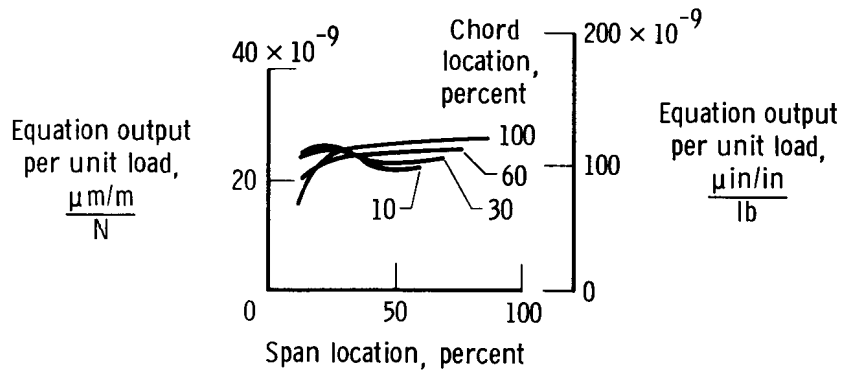


(f) Equation 93S.

Figure 8. Continued.

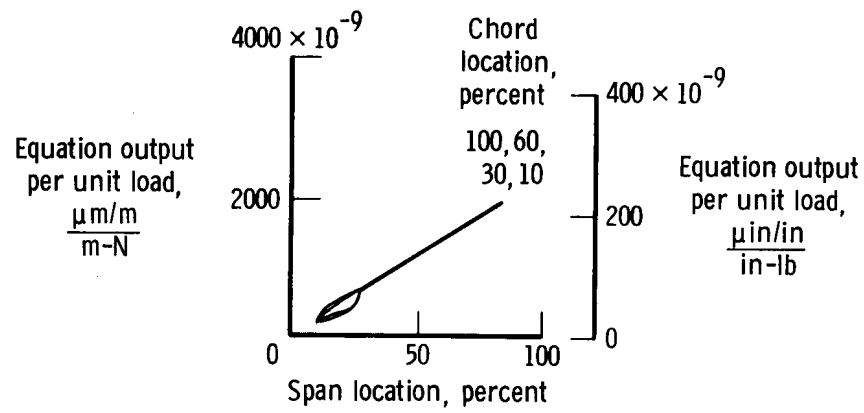


(g) Equation 94S.

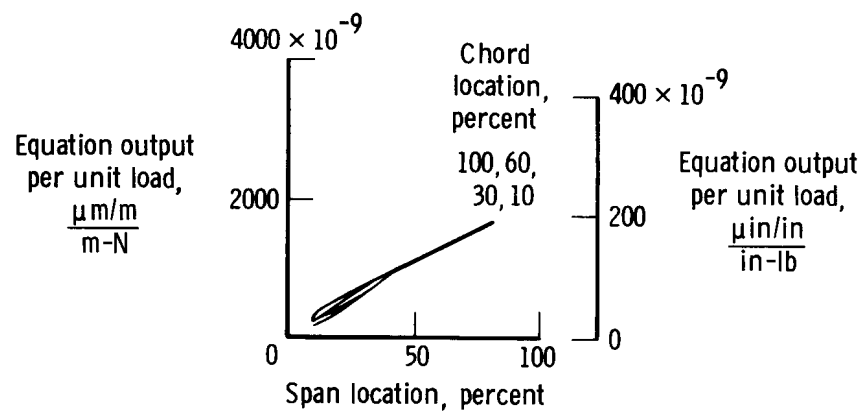


(h) Equation 95S.

Figure 8. Concluded.

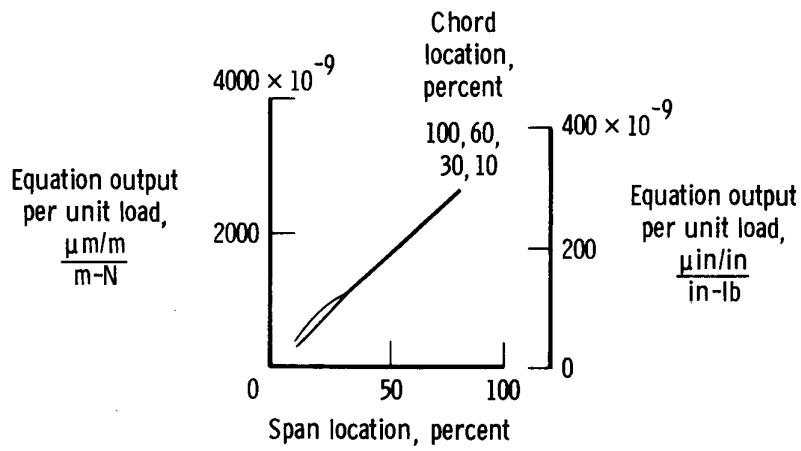


(a) Equation 80B.

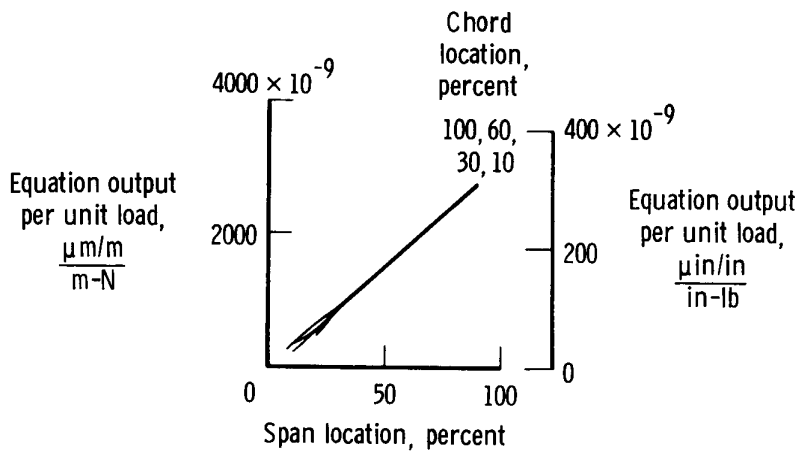


(b) Equation 81B.

Figure 9. Influence coefficient plots of bending moment equations.

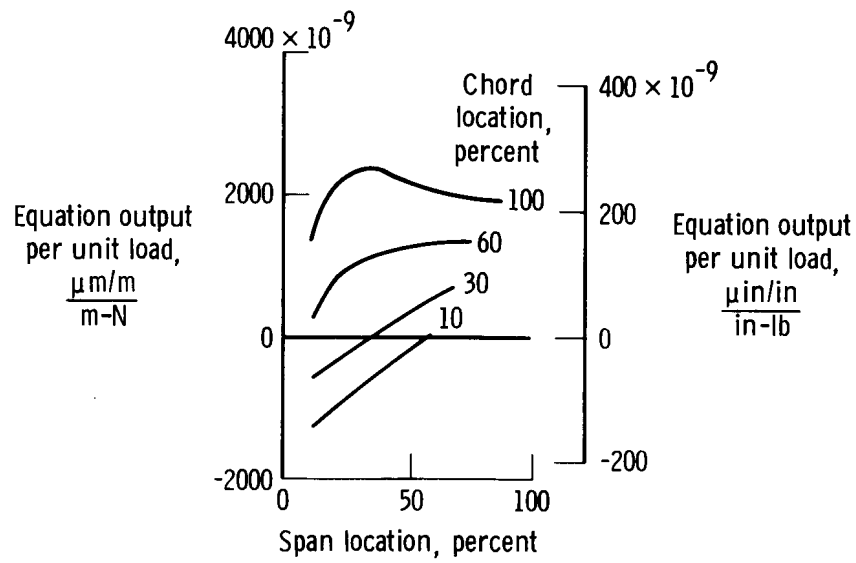


(c) Equation 82B.

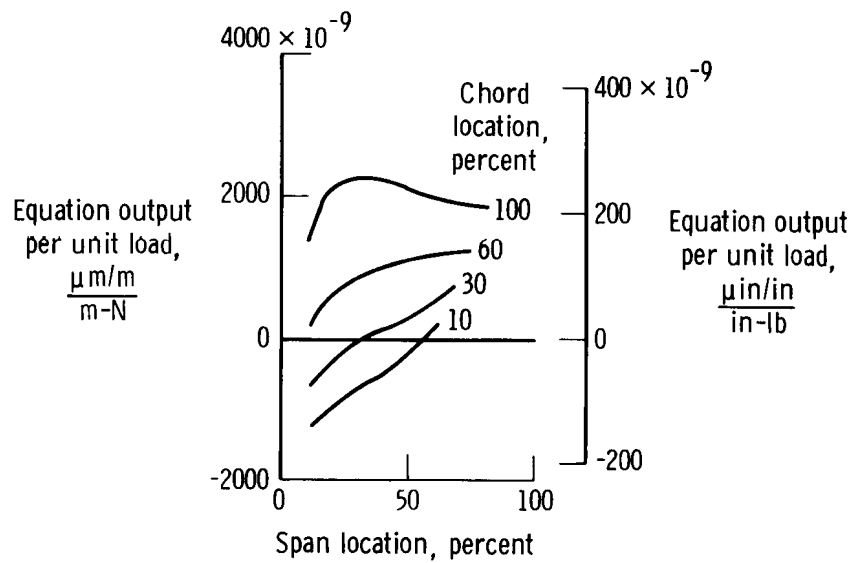


(d) Equation 83B.

Figure 9. Concluded.

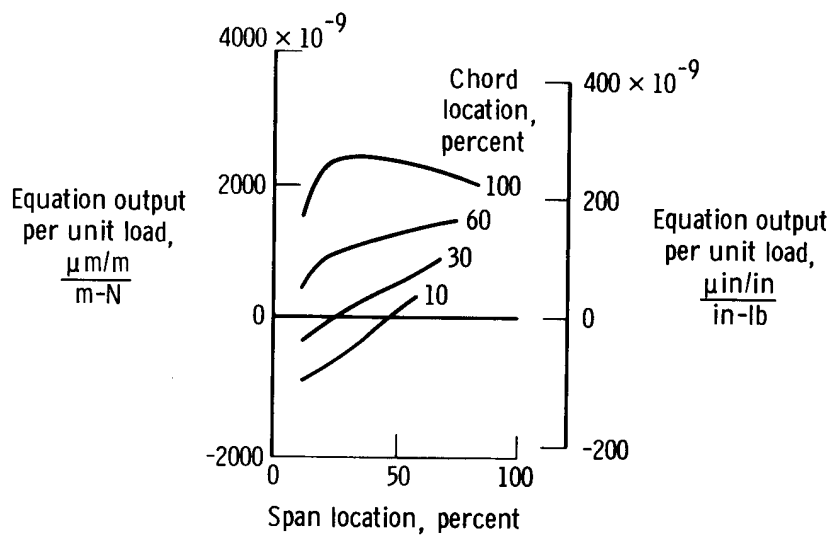


(a) Equation 84T.

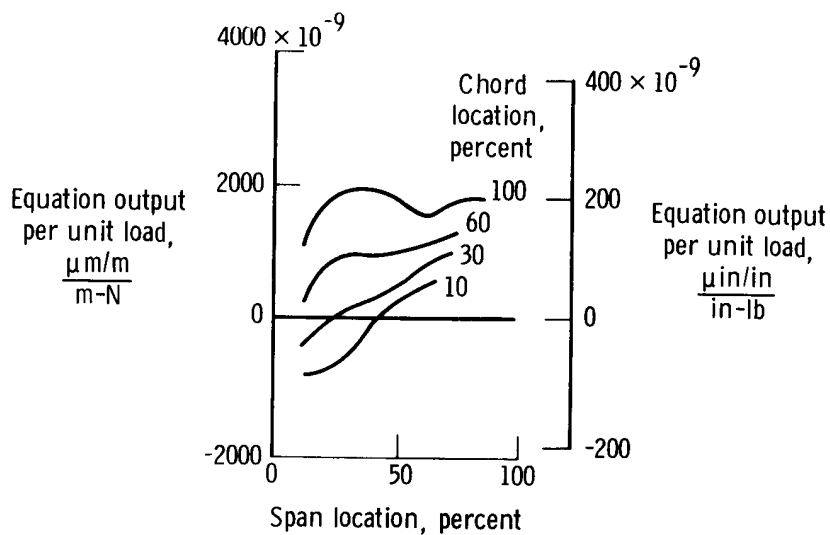


(b) Equation 85T.

Figure 10. Influence coefficient plots of torsion equations.

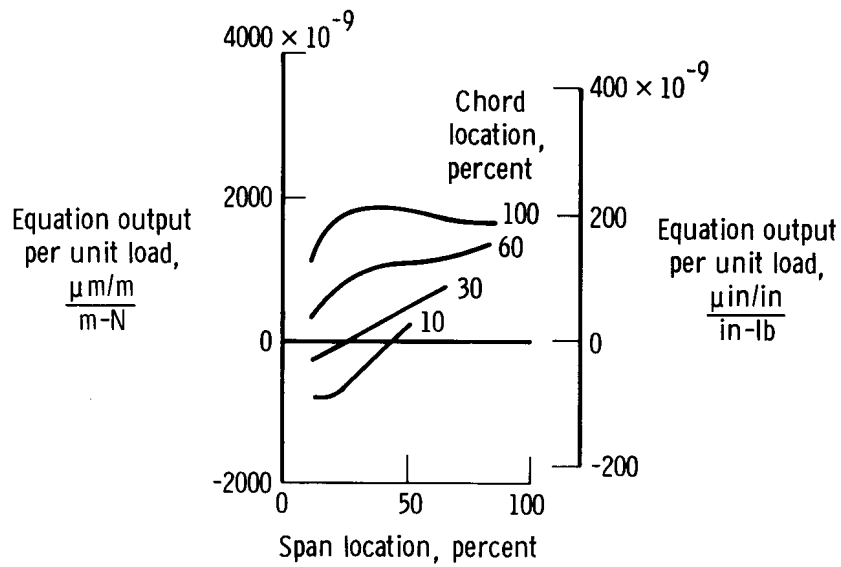


(c) Equation 88T.

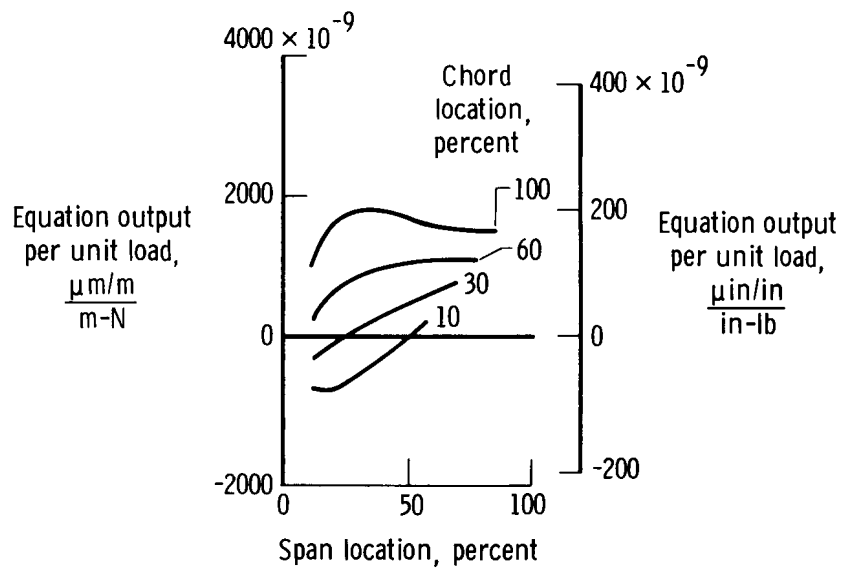


(d) Equation 89T.

Figure 10. Continued.

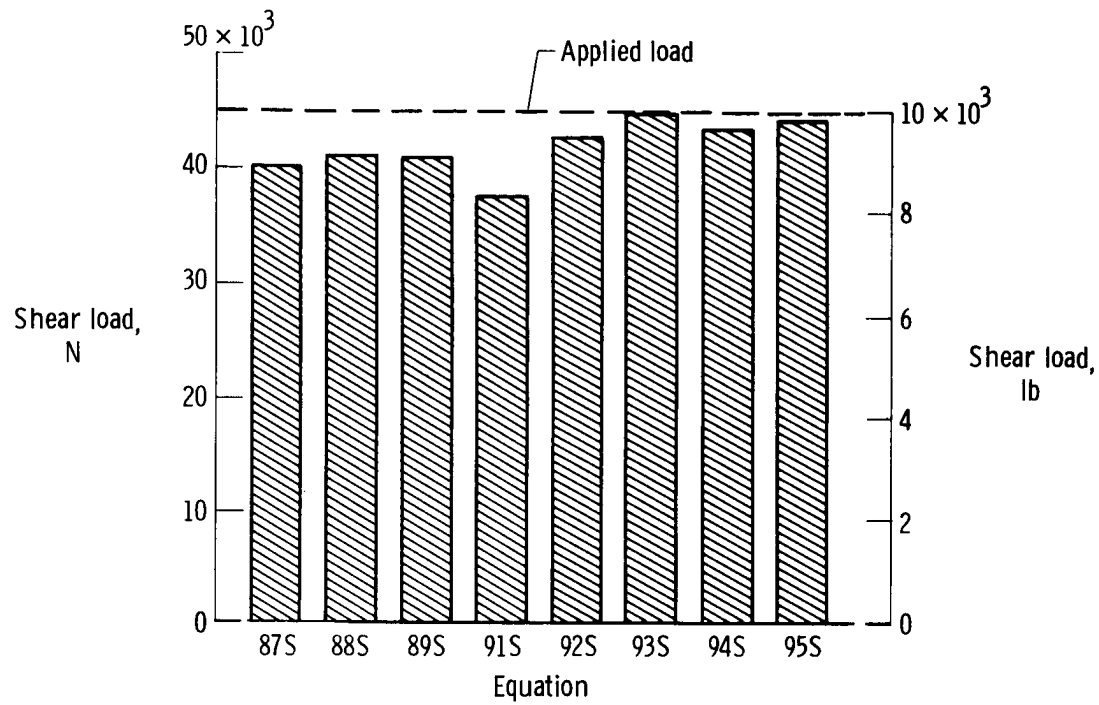


(e) Equation 90T.

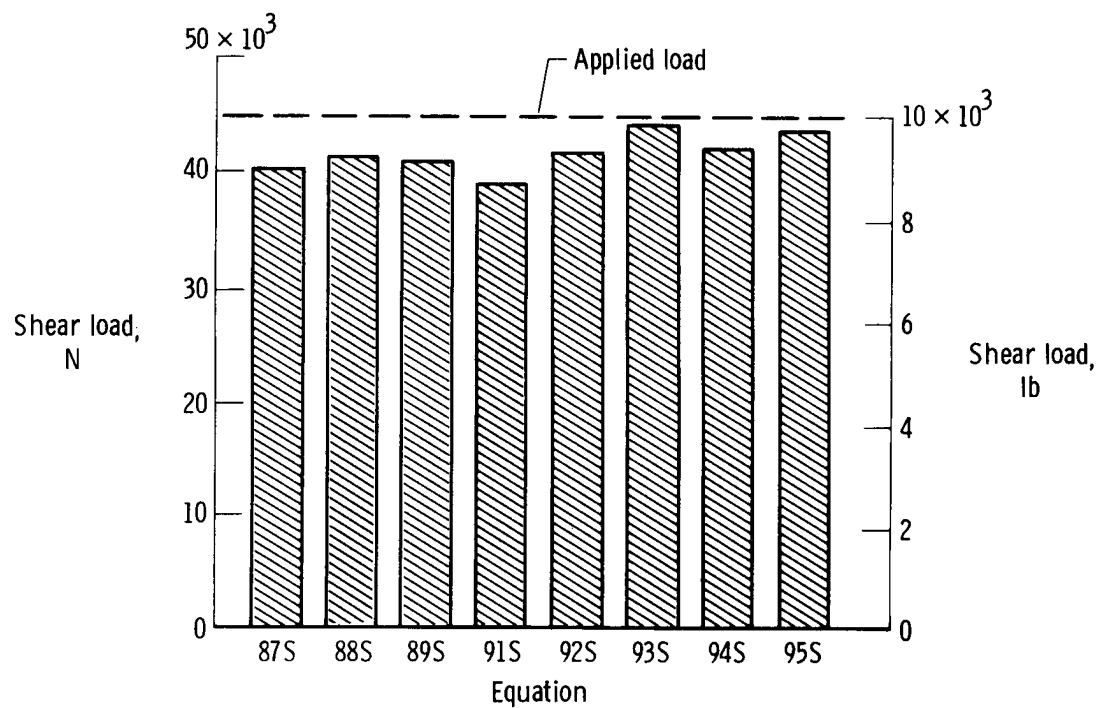


(f) Equation 91T.

Figure 10. Concluded.

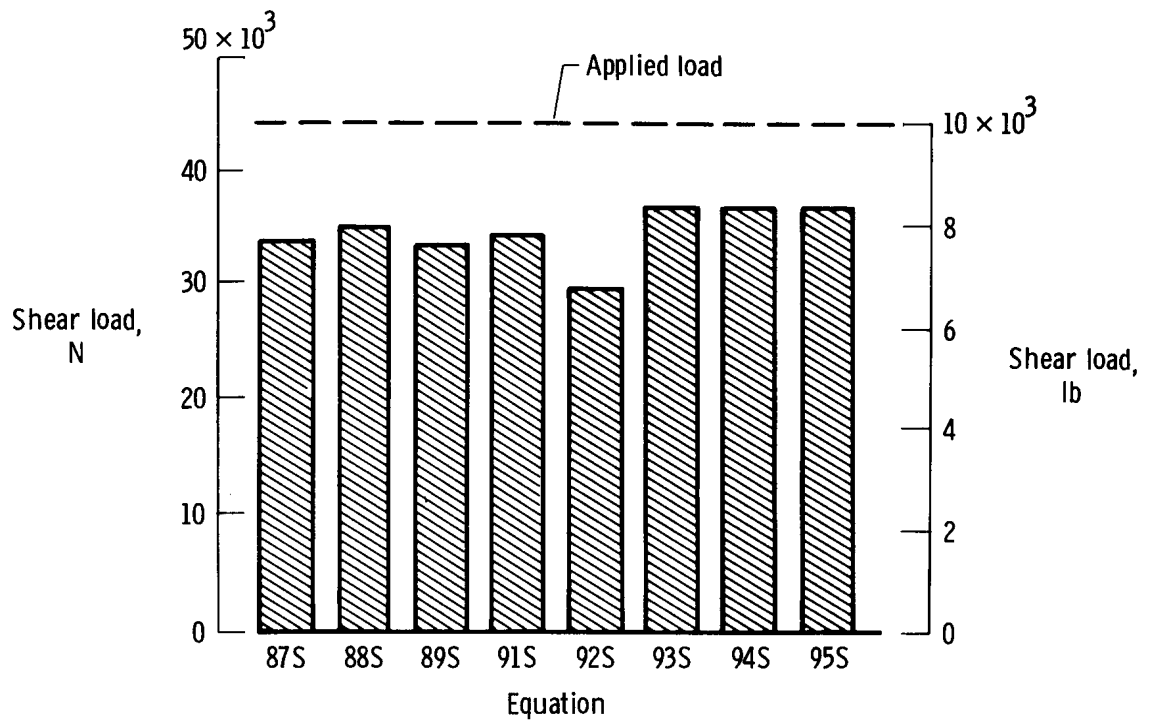


(a) Forward center of pressure loading.



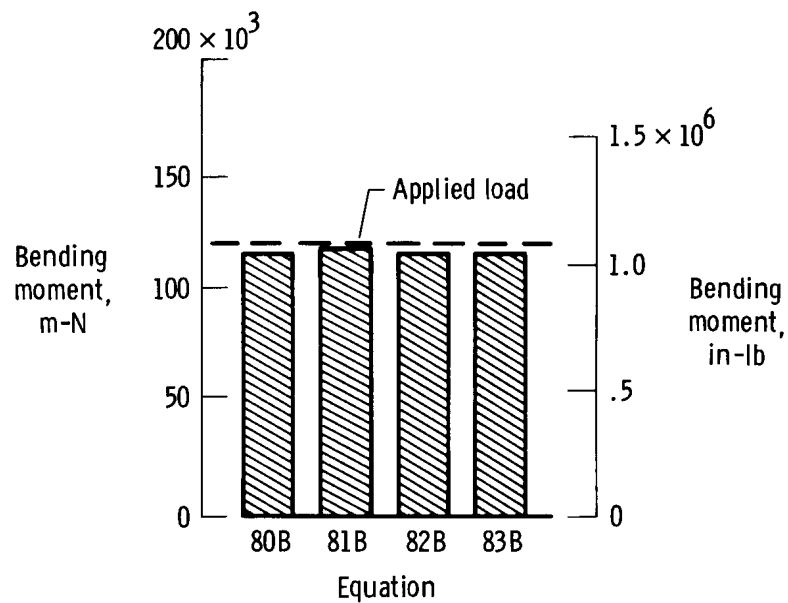
(b) Central center of pressure loading.

Figure 11. Comparison of calculated and mathematically applied shear loads.



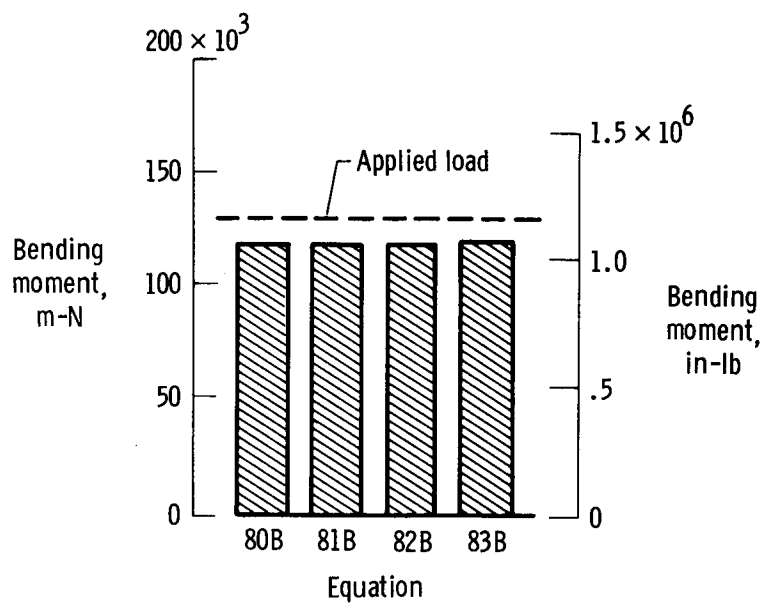
(c) Aft center of pressure loading.

Figure 11. Concluded.

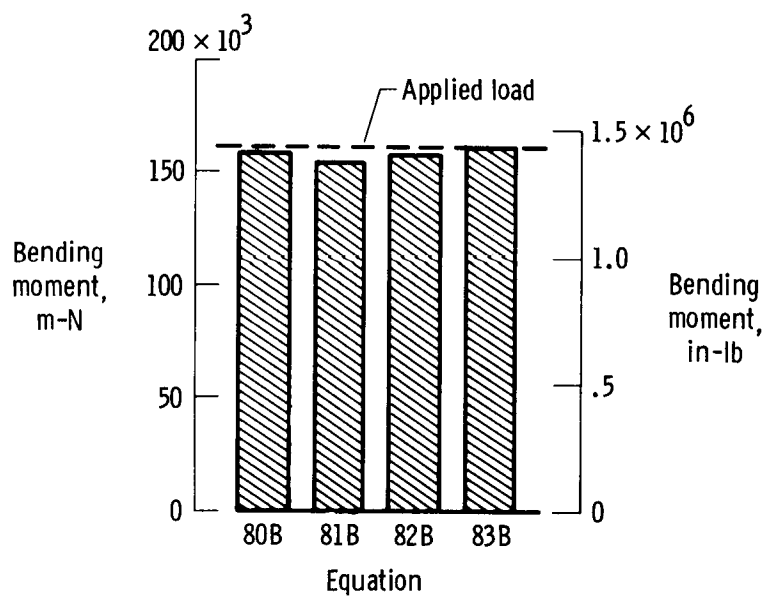


(a) Forward center of pressure loading.

Figure 12. Comparison of calculated and mathematically applied bending moments.

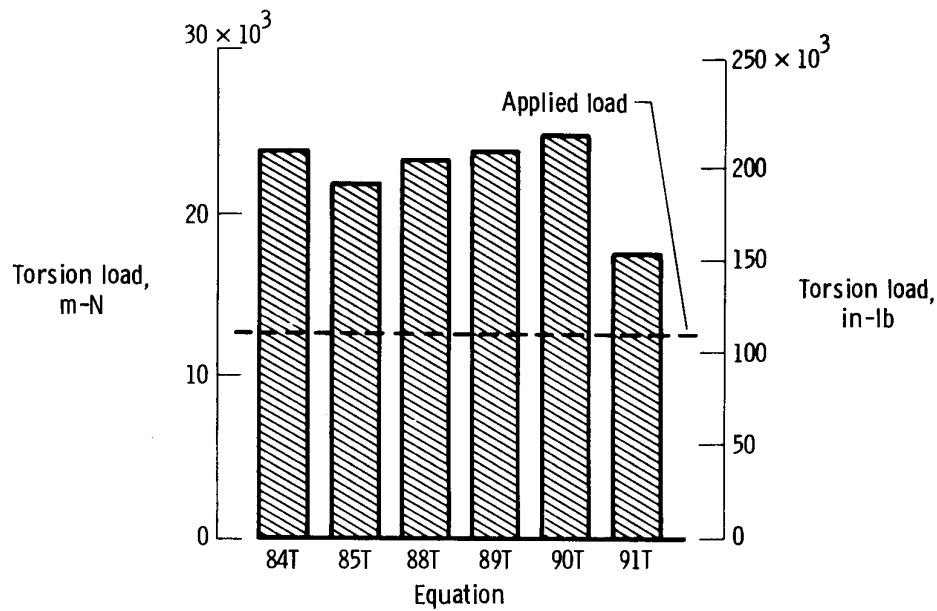


(b) *Central center of pressure loading.*

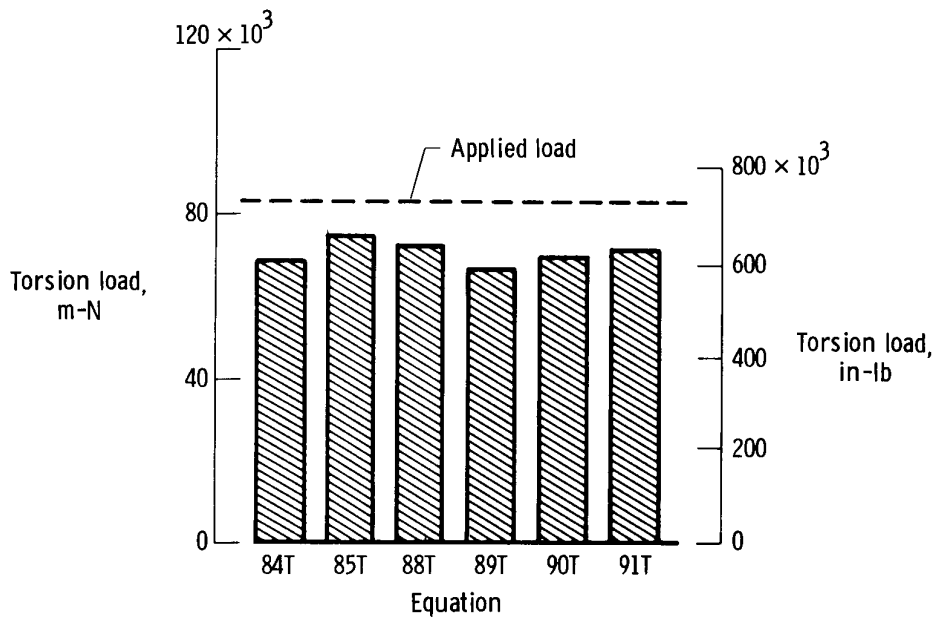


(c) *Aft center of pressure loading.*

Figure 12. Concluded.

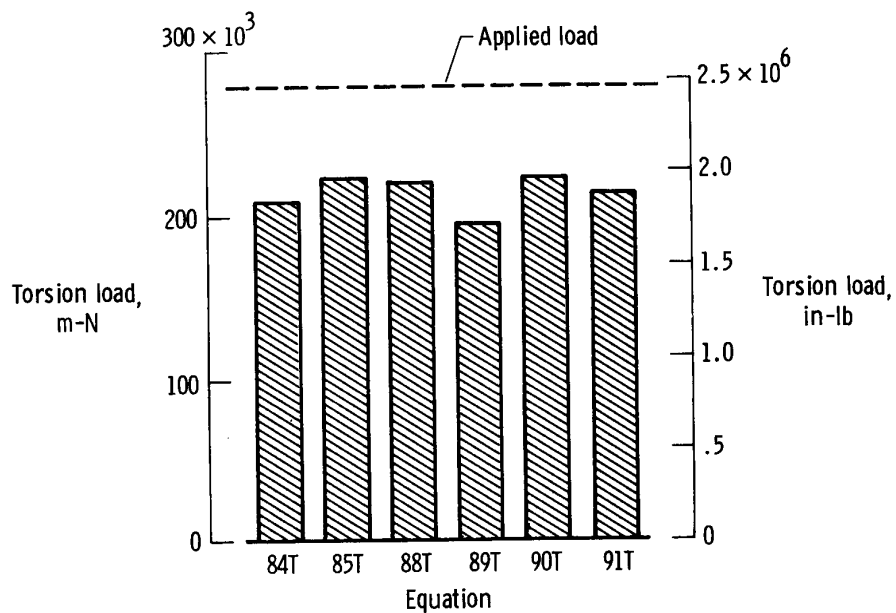


(a) Forward center of pressure loading.



(b) Central center of pressure loading.

Figure 13. Comparison of calculated and mathematically applied torsion loads.



(c) Aft center of pressure loading.

Figure 13. Concluded.

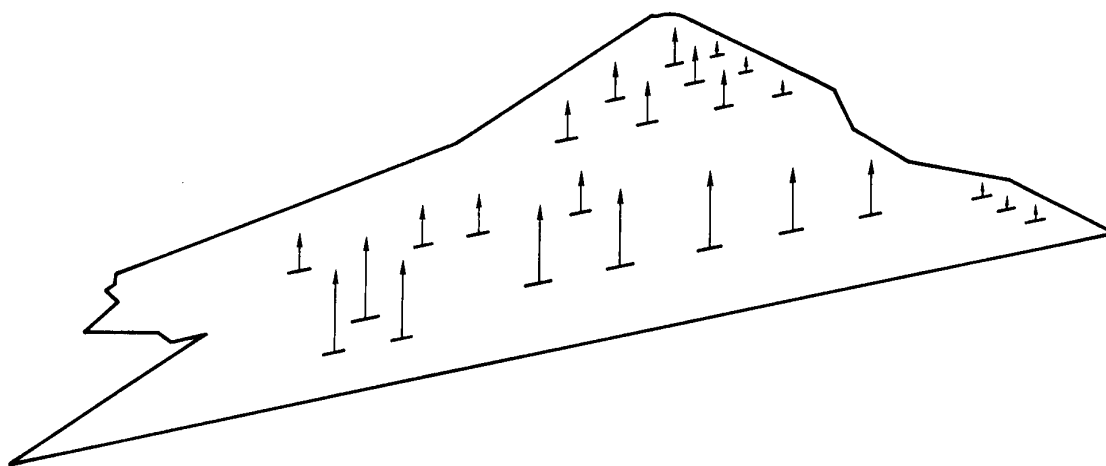


Figure 14. Location and relative magnitude of loads applied during load calibration.